Magnetic Resonance in Medicine 53:790–799 (2005)

Numerical Solution of the Bloch Equations Provides Insights Into the Optimum Design of PARACEST Agents for MRI

Donald E. Woessner,[1] Shanrong Zhang,[1] Matthew E. Merritt,[1] and A. Dean Sherry[1,2*]

Paramagnetic lanthanide complexes that display unusually slow water exchange between an inner sphere coordination site and bulk water may serve as a new class of MRI contrast agents with the use of chemical exchange saturation transfer (CEST) techniques. To aid in the design of paramagnetic CEST agents for reporting important biological indices in MRI measurements, we formulated a theoretical framework based on the modified Bloch equations that relates the chemical properties of a CEST agent (e.g., water exchange rates and bound water chemical shifts) and various NMR parameters (e.g., relaxation rates and applied B_1 field) to the measured CEST effect. Numerical solutions of this formulation for complex exchanging systems were readily obtained without algebraic manipulation or simplification. For paramagnetic CEST agents of the type used here, the CEST effect is relatively insensitive to the bound proton relaxation times, but requires a sufficiently large applied B_1 field to highly saturate the Ln^{3+}-bound water protons. This in turn requires paramagnetic complexes with large Ln^{3+}-bound water chemical shifts to avoid direct excitation of the exchanging bulk water protons. Although increasing the exchange rate of the bound protons enhances the CEST effect, this also causes exchange broadening and increases the B_1 required for saturation. For a given B_1, there is an optimal exchange rate that results in a maximal CEST effect. This numerical approach, which was formulated for a three-pool case, was incorporated into a MATLAB nonlinear least-square optimization routine, and the results were in excellent agreement with experimental Z-spectra obtained with an aqueous solution of a paramagnetic CEST agent containing two different types of bound protons (bound water and amide protons). Magn Reson Med 53: 790–799, 2005. © 2005 Wiley-Liss, Inc.

Key words: contrast agents; CEST imaging; PARACEST; Bloch theory; MRI

Most MRI contrast agents in clinical use or under current scientific investigation are based upon paramagnetic complexes that increase the relaxation rate (T_1 or T_2) of bulk water (1). Gadolinium (III) is widely used for this purpose because of the favorable magnetic (electron spin relaxation) and coordination (high coordination number and easy access of water to the inner coordination sphere) properties of complexes formed by this ion with a variety of ligands. An alternative and potentially powerful way to alter tissue contrast is to simply change the amount of water detected in an imaging experiment. Recently, Ward et al. (2) demonstrated that low-molecular-weight compounds with slowly exchanging –NH or –OH protons may also be used to alter tissue contrast via chemical exchange saturation transfer (CEST) of presaturated spins to bulk water. One important feature of this type of contrast agent is that one can switch the image contrast on or off at will by gating the RF presaturation pulse. For example, barbituric acid has two amide protons that resonate ~5 ppm downfield of bulk water. By applying a selective presaturation RF pulse at that frequency, the bulk water signal intensity can be reduced by ~30% in the presence of 125 mM barbituric acid, pH 7.4, 37°C (2). Although this amount of CEST agent is too high to be reasonably tolerated in vivo, the concept of using the CEST effect to alter tissue contrast is particularly attractive because it is based on entirely different intrinsic physical/chemical properties compared to the typical paramagnetic T_1 or T_2 shortening contrast agents. Goffeney and coworkers (3) demonstrated that the CEST effect can be amplified considerably by using macromolecules with a large number of chemically equivalent, exchangeable NH groups, and that the amide protons of intracellular proteins may be used in a CEST experiment to image tissue pH (4) or brain tumors (5).

Paramagnetic CEST analogs were not known until the recent discovery of lanthanide complexes that display unusually slow Ln^{3+}-bound water exchange kinetics (6,7). The first example was a EuDOTA-tetra(amide) complex that shows a highly shifted, bound water peak near 50 ppm in its high-resolution ^1H NMR spectrum in aqueous solution, even at 37°C (8). The water molecule in this complex has a bound lifetime ($\tau_M^{298} \sim 380$ μs) that is about 2000-fold longer than that of typical Gd^{3+} T_1 agents. This highly shifted bound water molecule may then be selectively labeled with the use of selective RF irradiation before an image is collected. Chemical exchange with bulk water during this presaturation period results in a decrease in bulk water signal intensity, and hence image contrast is proportional to chemical exchange. Paramagnetic CEST (PARACEST) agents have many potential advantages over intrinsic diamagnetic NH sites. First, much faster water or proton exchange systems can be used without approaching coalescence ($\Delta\omega^*\tau_M \leq 1$). We have shown that lanthanide complexes can be designed with a surprisingly wide range of τ_M and $\Delta\omega$ values (8). Second, the larger chemical shift allows the RF labeling pulse to be applied much farther away from the bulk water signal, leading to less off-resonance saturation of the bulk water signal. This is espe-

[1]Rogers Magnetic Resonance Center, Department of Radiology, University of Texas Southwestern Medical Center, Dallas, Texas.

[2]Department of Chemistry, University of Texas at Dallas, Richardson, Texas.

Grant sponsor: Robert A. Welch Foundation; Grant number: AT-584; Grant sponsor: National Institutes of Health; Grant numbers: CA-84697; RR-02584; Grant sponsor: Texas Advanced Technology Program.

*Correspondence to: A. Dean Sherry, Department of Chemistry, University of Texas at Dallas, P.O. Box 830688, Richardson, TX 75083-0688. E-mail: sherry@utdallas.edu

Received 18 August 2004; revised 8 October 2004; accepted 11 October 2004.

DOI 10.1002/mrm.20408
Published online in Wiley InterScience (www.interscience.wiley.com).

© 2005 Wiley-Liss, Inc.

15222594, 2005, 4, Downloaded from https://onlinelibrary.wiley.com/doi/10.1002/mrm.20408 by Weizmann Institute Of Science, Wiley Online Library on [26/11/2022]. See the Terms and Conditions (https://onlinelibrary.wiley.com/terms-and-conditions) on Wiley Online Library for rules of use; OA articles are governed by the applicable Creative Commons License

cially problematic in vivo, where the bulk water peak tends to be rather broad. Finally, since the CEST effect is intrinsically sensitive to chemical exchange, it should be relatively easy to design PARACEST agents to report important biological indices such as pH (9,10), temperature, O_2, redox state, and metabolite concentrations (11,12). The theoretical and experimental aspects of these paramagnetic CEST agents were recently reviewed (13). Zhou et al. (14) quantitatively described the proton exchange processes between water and solutes for CEST experiments by making several simplifying assumptions and approximations. In the present study, we formulated a theoretical framework (based on the Bloch equations modified to include chemical exchange) without simplifications to better understand how the chemical properties of a CEST agent (e.g., concentration and exchange rates) and the NMR parameters (e.g., chemical shifts, relaxation times T_1 and T_2, offset frequency, and strength of RF irradiation) affect CEST efficiency in a quantitative sense.

Modified Bloch Equations and the Numerical Approaches

CEST relies on the chemical exchange of nuclei between two or more different environments or "pools." This chemical exchange of nuclei carries the *X*, *Y*, and *Z* magnetizations of these nuclei from one pool to another—for example, between pool A (bulk water) and pool B (bound water). Their MR behavior can be fully described by the Bloch equations modified for chemical exchange (15,16).

$$\frac{dM_x^a}{dt} = -(\omega_a - \omega)M_y^a - k_{2a}M_x^a + C_bM_x^b \quad [1]$$

$$\frac{dM_x^b}{dt} = -(\omega_b - \omega)M_y^b - k_{2b}M_x^b + C_aM_x^a \quad [2]$$

$$\frac{dM_y^a}{dt} = (\omega_a - \omega)M_x^a - k_{2a}M_y^a + C_bM_y^b - \omega_1M_z^a \quad [3]$$

$$\frac{dM_y^b}{dt} = (\omega_b - \omega)M_x^b - k_{2b}M_y^b + C_aM_y^a - \omega_1M_z^b \quad [4]$$

$$\frac{dM_z^a}{dt} = \frac{M_0^a}{T_{1a}} - k_{1a}M_z^a + C_bM_z^b + \omega_1M_y^a \quad [5]$$

$$\frac{dM_z^b}{dt} = \frac{M_0^b}{T_{1b}} - k_{1b}M_z^b + C_aM_z^a + \omega_1M_y^b \quad [6]$$

where

$$k_{1a} = \frac{1}{T_{1a}} + C_a \quad [7]$$

$$k_{2a} = \frac{1}{T_{2a}} + C_a \quad [8]$$

and T_{1a} and T_{2a} are the relaxation times of pool A in the absence of exchange, ω is the frequency of the RF irradiation, ω_a is the Larmor frequency of pool A, ω_1 is the nutation rate of the RF irradiation (all ω terms are expressed in units of rad/s), and C_a is the transition rate of A spins leaving pool A (equal to $1/\tau_a$, where τ_a is the lifetime of a proton in pool A). Similar definitions apply to B spins. It is convenient to use the RF intensity $B_1 = \omega_1/2\pi$ expressed in Hz. The thermal equilibrium *Z* magnetizations, M_0^a and M_0^b, are directly proportional to the number of protons in pools A and B, respectively, as determined by the chemical composition of the system. Mass balance imposes the following relationship between the transition rates of both pools

$$C_a = \left(\frac{M_0^b}{M_0^a}\right)C_b = \left(\frac{M_0^b}{M_0^a}\right)\frac{1}{\tau_b} \quad [9]$$

Since PARACEST agents often have more than one type of exchangeable proton (as exemplified by the Eu^{3+}-water protons and the –NH protons of the EuDOTA-tetraamide complex shown in Scheme I), we also expanded the Bloch equations to a three-pool exchange case. The equations for the simplest three-pool case, formulated for exchange between pool A (bulk water) and pool B (Eu^{3+}-bound water), and between pool A (bulk water) and pool C (–NH), but not between pools B and C, include

$$\frac{dM_x^a}{dt} = -(\omega_a - \omega)M_y^a - k_{2a}M_x^a + C_bM_x^b + C_cM_x^c \quad [10]$$

$$\frac{dM_x^b}{dt} = -(\omega_b - \omega)M_y^b - k_{2b}M_x^b + C_{ab}M_x^a \quad [11]$$

$$\frac{dM_x^c}{dt} = -(\omega_c - \omega)M_y^c - k_{2c}M_x^c + C_{ac}M_x^a \quad [12]$$

$$\frac{dM_y^a}{dt} = (\omega_a - \omega)M_x^a - k_{2a}M_y^a + C_bM_y^b + C_cM_y^c - \omega_1M_z^a \quad [13]$$

$$\frac{dM_y^b}{dt} = (\omega_b - \omega)M_x^b - k_{2b}M_y^b + C_{ab}M_y^a - \omega_1M_z^b \quad [14]$$

$$\frac{dM_y^c}{dt} = (\omega_c - \omega)M_x^c - k_{2c}M_y^c + C_{ac}M_y^a - \omega_1M_z^c \quad [15]$$

$$\frac{dM_z^a}{dt} = \frac{M_0^a}{T_{1a}} - k_{1a}M_z^a + C_bM_z^b + C_cM_z^c + \omega_1M_y^a \quad [16]$$

$$\frac{dM_z^b}{dt} = \frac{M_0^b}{T_{1b}} - k_{1b}M_z^b + C_{ab}M_z^a + \omega_1M_y^b \quad [17]$$

$$\frac{dM_z^c}{dt} = \frac{M_0^c}{T_{1c}} - k_{1c}M_z^c + C_{ac}M_z^a + \omega_1M_y^c \quad [18]$$

In these equations, two new symbols appear because of the different chemical exchange dynamics: C_{ab} is the transition rate of pool A protons in leaving pool A and entering pool B, while C_{ac} is the transition rate of pool A protons in leaving pool A and entering pool C. Consequently,

15222594, 2005, 4, Downloaded from https://onlinelibrary.wiley.com/doi/10.1002/mrm.20408 by Weizmann Institute Of Science, Wiley Online Library on [26/11/2022]. See the Terms and Conditions (https://onlinelibrary.wiley.com/terms-and-conditions) on Wiley Online Library for rules of use; OA articles are governed by the applicable Creative Commons License

$$C_{ab} = \left(\frac{M_0^b}{M_0^a}\right) C_b \quad [19]$$

$$C_{ac} = \left(\frac{M_0^c}{M_0^a}\right) C_c \quad [20]$$

$$C_a = C_{ab} + C_{ac} \quad [21]$$

The definitions of C_i, k_{1i}, and k_{2i} remain as before. The Bloch equations for the general three-pool case in which exchange also occurs between pools B and C contain additional terms compared to those described above. The constraints on the exchange rate values imposed by mass balance require special attention, especially for use in a least-squares optimization.

In a typical CEST experiment, RF irradiation of intensity B_1 and frequency ω are applied until the steady-state condition is reached. At steady state, the time derivatives of Eqs. [1]–[6] (two-pool case) or Eqs. [10]–[18] (three-pool case) are equal to zero. The resulting set of six (or nine) simultaneous linear equations may be solved algebraically to obtain M_z^a/M_0^a for a selected range of irradiation frequencies and selected values of B_1. However, such a solution without algebraic simplification for more complex multipool systems (four pools or more with various different exchange pathways) seemed dauntingly laborious and error-prone. Therefore, we turned to numerical solutions.

As was done earlier in several calculations of NMR spectra for systems with multisite chemical exchange (17,18), we applied a standard method to solve sets of coupled equations (called Cramer's rule) to numerically solve the set of modified Bloch equations for the steady-state case. A QuickBasic program that utilizes the subroutine SIMLINEQ was written to implement Cramer's rule (the executable program is available on request) (19). The application of Cramer's rule simply involves writing the augmented matrix that contains the coefficients of *all* of the nuclear magnetizations and constant terms, such as M^a/T_{1a} and M^b/T_{1b} for the two-pool case. The numerical X, Y, and Z magnetizations for *all* pools of protons are included in the solution.

Experimentally, one may not know a priori the length of time required to reach steady state, so it would be useful to solve these equations without making that assumption. In this circumstance, one could solve the modified Bloch equations directly by using commercially available software with built-in ordinary differential equation (ODE) solvers (e.g., PSI-PLOT or MATLAB), but unfortunately this can be quite slow for large matrices and impractical for data fitting. However, these coupled equations are linear and can be rewritten into a more general format, $dY/dt = A*Y + b$, and solved analytically without further simplification with the use of the MATLAB built-in functions of matrix left division (\) and matrix power (expm 1) (see MATLAB 6.5.1 documentation for details). With these techniques, a three-pool case with nine OD equations may be solved within 1 s on a 750 MHz PC. The advantages of this method are that 1) it does not require the assumption of steady state (the length of the presaturation pulse is accounted for in the fitting of CEST spectra by the use of an exponential operator that expresses the time dependence of the equations), and 2) it becomes practical to implement a nonlinear least-squares optimization to fit experimental CEST data to exchange theory (the MATLAB program CESTFIT is available upon request).

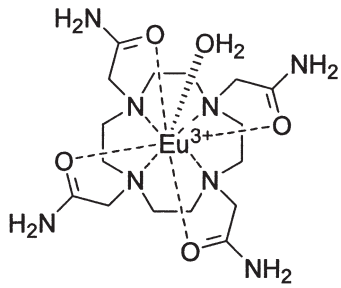

Scheme 1. The structure of EuDOTAM^{3+}.

MATERIALS AND METHODS

DOTAM (Scheme I) was synthesized using a published procedure (20). The europium (Eu^{3+}) complex of DOTAM was prepared by mixing solutions of the free ligand and $EuCl_3$ (1:1 mole ratio) at room temperature while maintaining the pH of the mixture near 7 by adding diluted NaOH as necessary. After maintaining these conditions with stirring for a few hours, free Eu^{3+} could no longer be detected using a standard colorimetric assay (xylenol orange in NaAc/HAc buffer at pH 5.3). The formation of the intact complex was confirmed by high-resolution ^{1}H NMR. A 10-mM aqueous solution of EuDOTAM in a 5-mm vial was positioned over the center of a 2-cm surface coil. Experimental CEST spectra (Z-spectra) were obtained with the use of a spin-echo pulse sequence modified by the addition of a frequency-selective presaturation pulse on a Varian 4.7T imaging system. The experimental Z-spectrum was obtained by integration of the water signal in a 1-mm coronal projection. The saturation frequency offset was arrayed between 20000 to –20000 Hz, with a step size of 200 Hz. A presaturation period of 2 s was used, and the presaturation RF power was varied from 15 to 40 db (corresponding to B_1 fields of 109 to 1020 Hz, respectively). All simulations and data fittings were performed on PCs with either PSI-PLOT version 7.5 (Poly Software Inc., Pearl River, NY) or MATLAB Release 13 (The Mathworks Inc., Natick, MA).

RESULTS AND DISCUSSION

Theoretical Considerations

In the most desirable situation, selective RF irradiation of the exchangeable CEST agent protons (pool B) should saturate these protons but not excite any of the bulk water protons (pool A). Chemical exchange causes a transfer of protons from pool A at a transition rate C_a equal to $1/\tau_a$, where τ_a is the lifetime of a proton in pool A. In that case, a proton that leaves A is replaced via chemical exchange with a proton that has zero Z magnetization. This exchange causes the Z magnetization to decrease at the rate $C_aM_z^a$ and results, in essence, in a magnetization drain from pool A from the initial value M_0^a to a new steady-state

15222594, 2005, 4, Downloaded from https://onlinelibrary.wiley.com/doi/10.1002/mrm.20408 by Weizmann Institute Of Science, Wiley Online Library on [26/11/2022]. See the Terms and Conditions (https://onlinelibrary.wiley.com/terms-and-conditions) on Wiley Online Library for rules of use; OA articles are governed by the applicable Creative Commons License

value, M_z^a. At the same time, the inherent spin-lattice relaxation of A protons (i.e., $[M_0^a - M_z^a]/T_{1a}$) tends to cause an increase in Z magnetization back toward the equilibrium value. The net rate of change of Z magnetization, dM_z^a/dt, is the difference between these two rates. At steady state, these two rates are equal, such that

$$C_a M_z^a = \frac{(M_0^a - M_z^a)}{T_{1a}} \qquad [22]$$

Rearrangement of Eq. [22] gives the steady-state value of M_z^a (also called the Z-value)

$$Z = \frac{M_z^a}{M_0^a} = \frac{\tau_a}{T_{1a} + \tau_a} \qquad [23]$$

The approach to steady state may be obtained by integrating dM_z^a/dt using M_0^a as the initial value at $t = 0$. This transient change is given by

$$\frac{M_z^a(t)}{M_0^a} = \frac{\tau_a}{T_{1a} + \tau_a} + \frac{T_{1a}}{T_{1a} + \tau_a} \exp\left(- \frac{T_{1a} + \tau_a}{T_{1a}\tau_a} t \right) \qquad [24]$$

The first term on the right-hand side is the steady-state value of Z. These simple relationships illustrate the key roles of small τ_a values and large T_{1a} values in minimizing Z.

To consider the potential influence of partial saturation of the bulk water spins (pool A) on the RF saturation of the pool B spins, it is instructive to consider the original Bloch equations (21) that describe a single pool of protons without chemical exchange. Here, RF irradiation at an offset frequency of ω_1 results in partial saturation to a new Z-value

$$\frac{M_z}{M_0} = \frac{1}{1 + \dfrac{\omega_1^2 T_1 T_2}{1 + \Delta\omega^2 T_2^2}}, \qquad [25]$$

where $\Delta\omega$ is the frequency difference between the applied RF irradiation and the Larmor frequency. Direct RF irradiated at the Larmor frequency ($\Delta\omega^2 = 0$) yields Eq. [26], which indicates that the strength of the RF irradiation, ω_1 ($= 2\pi B_1$), plays a key role in the degree of saturation of the bound protons.

$$\frac{M_z^b}{M_0^b} = \frac{1}{1 + \omega_1^2 T_{1b} T_{2b}} \qquad [26]$$

Although large values of B_1 enable the highest degree of saturation of B protons, the use of a large B_1 value can obscure the true CEST effect by causing direct excitation of A protons unless there is a large chemical shift between these pools. An illustration of the off-resonance excitation of bulk water protons brought about by irradiation of protons at site B, 475 Hz away from a second site (site A), can be shown with a non-exchanging system with $T_{1b} = T_{2b} = 0.01$ s and $T_{1a} = T_{2a} = 1$ s. As previously noted by Zhou et al. (14), only when B_1 approaches infinity does pool B approach the saturation state. However, Eq. [26] predicts that 99.9% of B spins (virtually complete saturation) can be saturated with a B_1 of only 503 Hz. This value is easily generated by conventional NMR spectrometers. A "nominal" 99% saturation requires only 158 Hz. Equation [25] predicts that applying a $B_1 = 158$ Hz directly to pool B will result in 10% saturation (i.e., $M_z^a/M_0^a = 0.90$) of pool A, even for pool A protons that resonate only 475 Hz away from pool B protons. This frequency difference corresponds to a chemical shift difference of 7.5 ppm at 1.5T, or 2.4 ppm at 4.7T. Thus, this simple non-exchanging case demonstrates that off-resonance excitation of bulk water protons is an important consideration in the evaluation of quantitative CEST effects. Thus, PARACEST agents with large $\Delta\omega$ values have a major advantage over diamagnetic CEST agents in that off-resonance effects can be minimized.

Even in the absence of chemical exchange, the strategy of minimizing off-resonance irradiation of bulk water protons by the use of small B_1 values requires a PARACEST agent with long T_{1b} and T_{2b} values (Eq. [26]). Once chemical exchange is allowed (a fundamental requirement of CEST), this effect is further exacerbated because exchange broadening decreases the value of T'_{2b}, the apparent transverse relaxation time. In the limiting case in which $\tau_b \gg 1/(2\pi\,\Delta\nu)$, where $\Delta\nu$ is the Larmor frequency shift between A and B protons, it is well known (16) that exchange broadening effectively shortens T'_{2b} to

$$\frac{1}{T'_{2b}} = \frac{1}{T_{2b}} + \frac{1}{\tau_b} \qquad [27]$$

where T_{2b} is the transverse relaxation time that could be measured if the exchange did not occur. This would not only decrease the saturation of the pool B protons, but would also cause an increase in the frequency range of direct excitation of the pool A protons. Even shorter τ_b values would result in less saturation of B protons, but would also further facilitate the Z magnetization drain from the A protons. It follows then that there is an optimal τ_b lifetime (vide infra).

Simulations for a Two-Pool Model

Figures 1 and 2 illustrate the influence of chemical exchange on saturation efficiency in a two-pool PARACEST experiment. The top panel of Fig. 1 shows that if pool B (20 mM) is in relatively slow exchange with bulk water, $C_b = 500\ s^{-1}$, it can be fully saturated with the use of a B_1 of 512 Hz (the thin line). After steady-state exchange with bulk water spins, this would result in a 15.3% decrease in the intensity of pool A (the thick line), as predicted by Eq. [23]. However, a system with $C_b = 500\ s^{-1}$ corresponds to a PARACEST agent with an Ln^{3+}-bound water lifetime (τ_M) of 2 ms, a value that may be difficult to achieve experimentally (7). The bottom panel shows the effect of using a PARACEST agent with an experimentally attainable τ_M value of 200 μs (7) ($C_b = 5{,}000\ s^{-1}$). Again, after steady-state exchange, this would result in greater saturation of the bulk water signal (34.8%), but less than that predicted by Eq. [23] (the predicted result is 64.5%). The reason for this difference is that in this case, an applied B_1 field of 512 Hz is not powerful enough to fully saturate the

15222594, 2005, 4, Downloaded from https://onlinelibrary.wiley.com/doi/10.1002/mrm.20408 by Weizmann Institute Of Science, Wiley Online Library on [26/11/2022]. See the Terms and Conditions (https://onlinelibrary.wiley.com/terms-and-conditions) on Wiley Online Library for rules of use; OA articles are governed by the applicable Creative Commons License

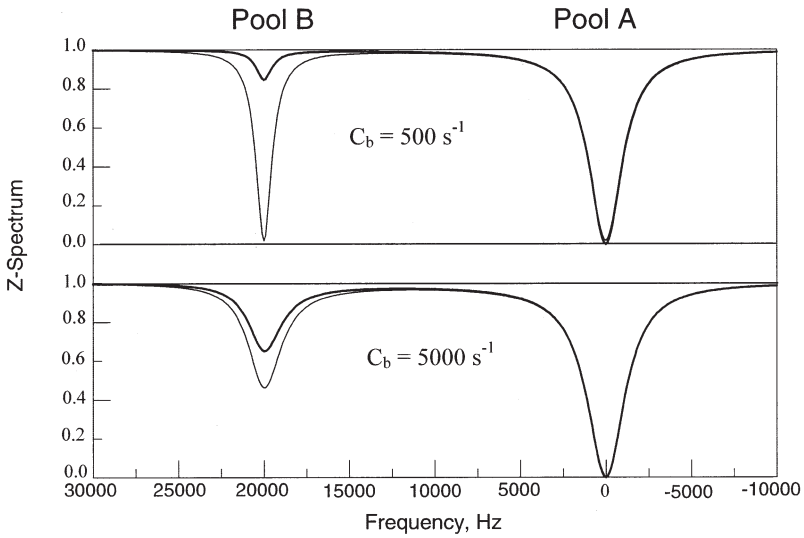

FIG. 1. Simulated *Z*-spectra for a two-pool exchange system with bulk water (pool A) at zero and bound water (pool B) at 20000 Hz, illustrating the differences between slow (C_b = 500 s^{-1}) and fast (C_b = 5000 s^{-1}) exchanging systems. The thin line peak centered at 20000 Hz in each panel shows the amount of pool B spins saturated by a 512 Hz B_1 pulse of long duration. The thick line peak centered at 20000 Hz shows the net decrease in bulk water intensity (M_z^a/M_0^a) after a steady-state exchange between the irradiated B spins and the A spins. The remaining parameters used in this simulation include: T_{1a} = 1 s, T_{2a} = 0.2 s, T_{1b} = 0.1 s, T_{2b} = 0.1 s, and M_0^b/M_0^a = 0.0003636.

rapidly exchanging pool B spins (the thin line). This demonstrates that Eq. [23] should not be used for quantitative purposes in situations where the pool B spins are not highly saturated by the applied B_1 field. Simulations show that for a given value of C_b, the degree of saturation monotonically increases as B_1 is increased up to very large value. Thus, one could of course increase B_1 to a value that would fully saturate all pool B spins, but this would then amplify the effects of indirect irradiation of pool A spins (described above). Also, Fig. 2 illustrates that for a given B_1 value, the steady-state residual Z magnetization of pool A following irradiation of the pool B spins passes through a broad minimum when $C_b = 2\pi B_1$ (shown as an inset in the figure). This important relationship allows one to predict a priori the optimum C_b value needed to produce an optimal CEST effect for any given B_1 value. The B_1 can be chosen to achieve a "balance" between the opposing requirements of minimal residual Z magnetization and minimal indirect irradiation of pool A while staying within instrumental RF power capabilities and following medical guidelines for irradiation power. This should ultimately allow one to choose the optimum PARACEST agent from a group of agents with known bound water lifetimes.

Figure 3 illustrates the large influence of the relaxation times of pool A on *Z*-spectra. The top panel shows the effect of increasing T_{1a} on increasing the CEST efficiency (the amount of decrease in Z that results from chemical exchange) at the frequency of pool B, as suggested by Eq. [23]. The decreases in Z in the region of the bulk water frequency with increasing T_{1a} show the increasing effect of off-resonance excitation of bulk water protons, as suggested by Eq. [25]. The bottom panel illustrates the influence of changes in T_{2a} on the Z-spectrum in the frequency region around that of the bulk water and in the region between the two resonance peaks. This is especially pertinent to applications of PARACEST agents in vivo, where tissue water may have a rather short T_2. This figure illustrates that while CEST efficiency is not dramatically affected by changes in T_{2a}, the off-resonance "indirect" irradiation of pool A becomes more problematic. This again

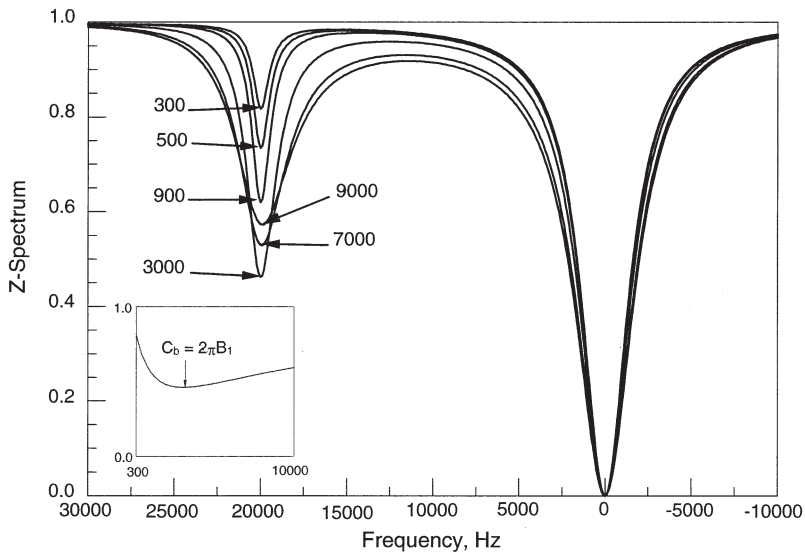

FIG. 2. Simulated two-pool *Z*-spectra showing the effects of different values of exchange rate, C_b, of the bound water on the Z value at the bound water frequency. The values of the parameters are the same as in Fig. 1, except that T_{1a} = 2 s. The C_b values, in units of s^{-1}, are indicated in the graph. The inset shows a plot of the Z value after irradiation is applied at the bound water frequency as a function of C_b, varied from 300 s^{-1} to 10000 s^{-1}. The minimum Z value occurs when the exchange rate, C_b, equals $2\pi B_1$.

15222594, 2005, 4, Downloaded from https://onlinelibrary.wiley.com/doi/10.1002/mrm.20408 by Weizmann Institute Of Science, Wiley Online Library on [26/11/2022]. See the Terms and Conditions (https://onlinelibrary.wiley.com/terms-and-conditions) on Wiley Online Library for rules of use; OA articles are governed by the applicable Creative Commons License

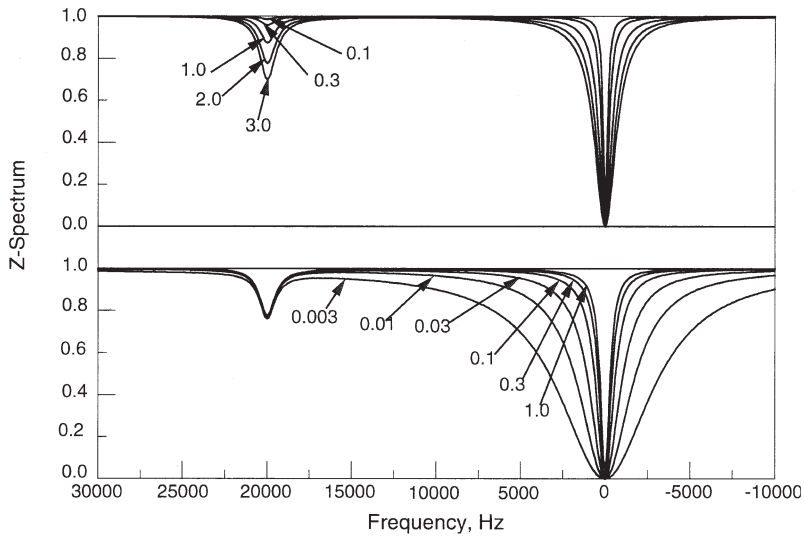

FIG. 3. Simulated two-pool *Z*-spectra showing the dependencies of *Z* on the T_{1a} and T_{2a} values. The upper graph is for T_{2a} = 0.1 s and various T_{1a} values in units of s, as indicated in the graph. The lower graph is for T_{1a} = 2 s and various T_{2a} values in units of s, as indicated in the graph. The other parameters are fixed as T_{1b} = 0.1 s, T_{2b} = 0.08 s, C_b = 3000 s^{-1}, M_0^b/M_0^a = 0.0007272, and B_1 = 128 Hz.

emphasizes the importance of PARACEST agents having highly shifted bound water resonances (large Δω). Conversely, the relaxation times of pool B protons have a much smaller influence on the *Z*-spectra (simulations not shown). This feature may also play a role in the design of an optimal paramagnetic CEST agent because the paramagnetic ions that induce the largest shifts in the bound water resonance are typically the same ions that relax those protons most efficiently (i.e., Tb^{3+}, Dy^{3+}).

Simulations for a Three-Pool Model

The two-pool simulations serve to illustrate the consequences of the relaxation times and chemical exchange. However, most CEST experiments will involve more than one pool of exchangeable protons, and this feature introduces additional effects to the *Z*-spectrum. Exchangeable amide NH protons comprise a second type of bound protons in typical PARACEST agents. For a EuDOTA-tetraamide complex, such as that illustrated in Scheme I, such NH protons commonly have chemical shifts around –5 ppm from the bulk water protons and form only a shoulder on the bulk water peak in the *Z*-spectrum. To clearly illustrate the effects of a third pool on the *Z*-spectrum, it is useful to simulate the case in which both pools of exchangeable protons have large chemical shifts away from bulk water. Figure 4 shows simulations of a three-pool case in which the bulk water undergoes proton exchange with each of two pools of protons, neither of which exchanges directly with each other. In this simulation, the T_{1c} and T_{2c} values of the third pool (C) are much smaller than those of pool B. Interestingly, the residual *Z* magnetization at pool B (20000 Hz) is dramatically affected by the increased rate of exchange between pools C and A because of several different effects. First, exchange with pool C can decrease the CEST effect by replacing A protons with protons that may have less saturation than pool A itself. Also, in this example, a more rapid exchange between sites C and A results in an effective decrease in T_{1a}, which reduces the amount of CEST observed resulting from irradiation of pool B. Furthermore, indirect chemical

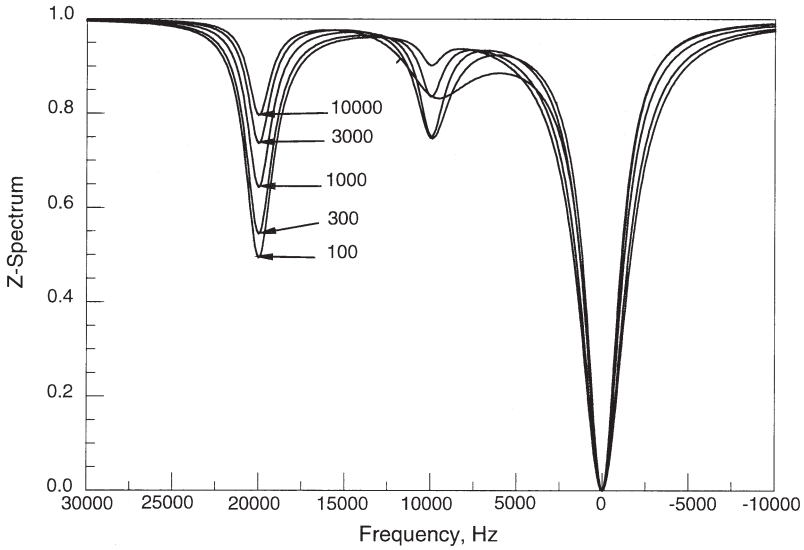

FIG. 4. Simulated three-pool *Z*-spectra showing the increase in the *Z* value at the bound water frequency with an increase in the exchange rate of protons in the third pool (pool C) with a short T_1 value. The parameters are T_{1a} = 2 s, T_{2a} = 0.2 s, T_{1b} = 0.1 s, T_{2b} = 0.1 s, C_b = 3000 s^{-1}, M_0^b/M_0^a = 0.0003636, and B_1 = 512 Hz. The parameters of pool C, at 10000 Hz, are T_{1c} = 0.3 ms, T_{2c} = 0.3 ms, and M_0^c/M_0^a = 0.0007272. The exchange rates C_c in s^{-1} are given in the graph.

15222594, 2005, 4, Downloaded from https://onlinelibrary.wiley.com/doi/10.1002/mrm.20408 by Weizmann Institute Of Science, Wiley Online Library on [26/11/2022]. See the Terms and Conditions (https://onlinelibrary.wiley.com/terms-and-conditions) on Wiley Online Library for rules of use; OA articles are governed by the applicable Creative Commons License

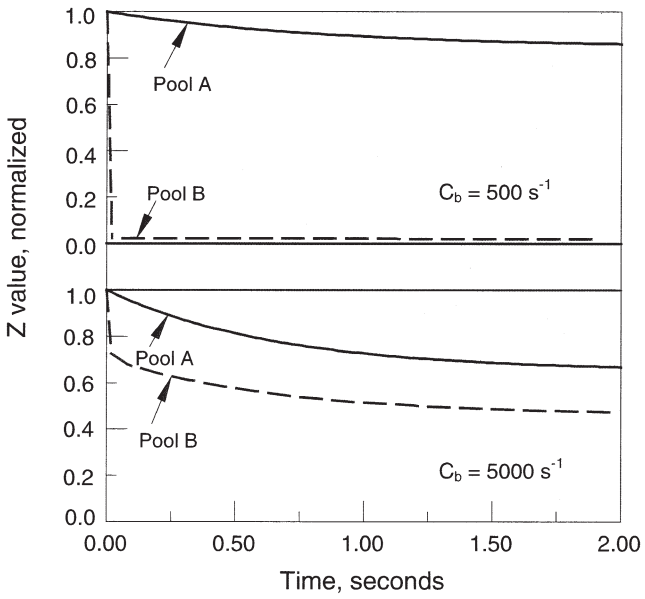

FIG. 5. Simulated approach to steady state for the two-pool systems using the NMR parameters of Fig. 1. The irradiation is applied at the frequency of the bound water (pool B). The dashed lines are the M_z^b/M_0^b values. The upper graph is for slow exchange, C_b = 500 s^{-1}. The lower graph is for rapid exchange, C_b = 5000 s^{-1}. The T_{ss} (simulated) values obtained from analysis of the simulated Z spectra are 0.847 s (upper graph) and 0.652 s (lower graph). The T_{ss} (calculated) values obtained from Eq. [28], which assumes complete saturation of pool B protons (i.e., Z_b = 0), are 0.846 s (upper) and 0.652 s (lower). The calculated lifetimes obtained by insertion of these T_{ss} (simulated) values into Eq. [28] are 2.015 ms (upper) and 0.679 ms (lower). The corresponding "true" lifetimes are 2.000 ms (upper) and 0.200 ms (lower). These results show that a high degree of saturation, obtained by using a large B_1 value, is necessary to obtain the values predicted by Eqs. [23] and [28].

exchange of protons between pools B and C (via pool A) lowers the effective T_{1b} value and causes less saturation of B protons (as shown by simulations), thereby further reducing the CEST effect.

Approach to Steady State

The time required to apply the RF irradiation to the sample so as to attain the steady-state condition can be calculated by obtaining the numerical solution to the appropriate set of coupled linear first-order homogeneous differential equations (Eqs. [1]–[6] for the two-pool case, and Eqs. [10]–[18] for the three-pool case) without algebraic simplification, starting at the beginning of the application of the RF irradiation. In this way, the time dependences of the numerical X, Y, and Z magnetizations for *all* of the pools of protons can be obtained. The time-dependent Z values shown in this paper were obtained with the ODE solver in commercial mathematical software PSI-PLOT (MATLAB gave similar values). Figure 5 shows the approach to steady state for the two-pool cases of Fig. 1. The depicted Z values are obtained when the irradiation is applied at the frequency of the bound water (pool B). Equation [24], which gives the transient approach to steady state for the ideal case in which the bound protons have zero Z magnetization, predicts that the steady-state M_z^a value given by Eq. [23] is approached exponentially with a time constant T_{ss} given by

$$T_{ss} = \frac{T_{1a}\tau_a}{T_{1a} + \tau_a} \qquad [28]$$

The τ_a value can be expressed in terms of τ_b and CEST agent concentration with the use of Eq. [9].

The T_{ss} (calculated) values described in the legend of Fig. 5 were obtained by the use of Eqs. [9] and [28] together with the T_{1a} and C_b values listed. The T_{ss} (simulated) values are obtained by fitting the simulated curves to a single exponential decay. The top panel, with the relative slow exchange of bound water (C_b = 500 s^{-1}) and nearly complete saturation of pool B, shows that the T_{ss} (simulated) value is nearly identical to T_{ss} (calculated). On the other hand, the bottom panel, in which pool B is only about one-half saturated, shows that the T_{ss} (simulated) value is much larger than the T_{ss} (calculated) value (0.652 s vs. 0.355 s).

One can also estimate the τ_b value by using T_{ss} and T_{1a}, and Eqs. [9] and [28]. In the top panel, with nearly complete saturation of pool B, the estimated τ_b value (2.015 ms) is very close to the "actual" value (2.000 ms). In the bottom panel, however, the estimated value of τ_b (0.679 ms) is several times greater that the "actual" value (0.200 ms). These results show that an estimation of bound water lifetime obtained from a measured approach to steady state, the T_{1a} and CEST agent concentration, together with Eqs. [28] and [9], can be in error if the bound water protons are not highly saturated. This is shown more clearly in Fig. 6, in which the estimated bound water lifetime (τ_b) is plotted as a function of degree of saturation of pool B protons. These results show that if the degree of saturation (varied by changing B_1) falls much below ~90%, the estimated τ_b value becomes increasingly greater than the "actual" value of 1 ms. This was observed experimentally in a previous study (8).

Using simulations (employing the numerical solutions to the complete modified Bloch equations) of the approach to steady state to analyze experimental measurements should be more accurate than applying Eq. [28] to the data because the derivation of Eq. [28] assumes that the pool B protons are completely saturated. The present method does not make this assumption.

Fitting Experimental CEST Spectra

Shown in Fig. 7 are the experimental (data points) and the best-fitted (curves) CEST spectra of a 10-mM aqueous solution of $EuDOTAM^{3+}$ at four different B_1 values, respectively. The identical initial, upper, and lower boundary values were used for τ_M (10–200 μs for Eu^{3+}-H_2O and 100–1500 μs for NH), δ (40–70 ppm for Eu^{3+}-H_2O, –3 to –10 ppm for NH), T_{1A} (0.01–5 s) and T_{2A} (0.01–5 s), respectively. Since the relaxation times of the bound pools were insensitive (as demonstrated by simulations), these values were fixed in the optimization to $T_{1B} = T_{1C}$ = 1.0 s, and $T_{2B} = T_{2C}$ = 0.2 s, respectively. The fitting algorithm does not require an assumption of complete saturation or attainment of a steady-state condition; rather, the presaturation pulse length was

15222594, 2005, 4, Downloaded from https://onlinelibrary.wiley.com/doi/10.1002/mrm.20408 by Weizmann Institute Of Science, Wiley Online Library on [26/11/2022]. See the Terms and Conditions (https://onlinelibrary.wiley.com/terms-and-conditions) on Wiley Online Library for rules of use; OA articles are governed by the applicable Creative Commons License

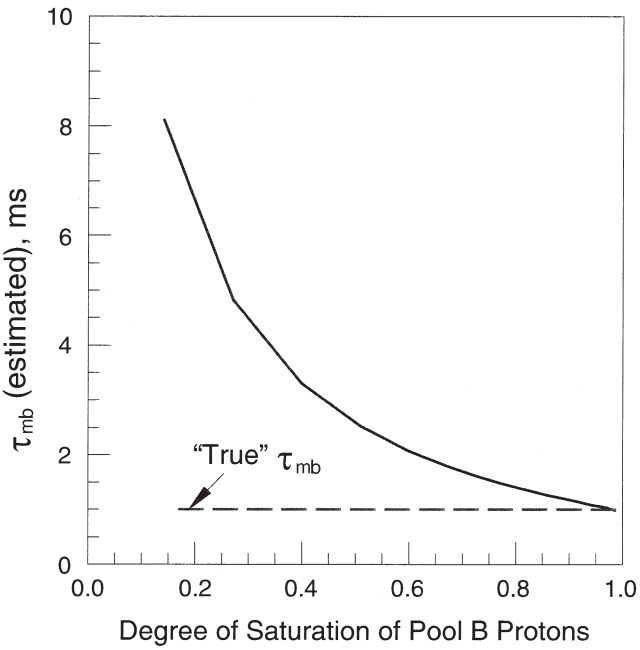

FIG. 6. The dependence of estimated bound proton lifetimes, τ_{Mb} (estimated), on the degree of saturation, $(1 - M_z^b/M_0^b)$, obtained from the simulations of the approach to steady state. This graph shows the effect of the degree of saturation of the bound water protons on the estimated bound proton lifetimes, and illustrate that a high degree of saturation is required for the error of the estimated lifetime to be small. The degree of saturation of pool B protons was changed by varying B_1 from 50 Hz to 1000 Hz. The remaining parameters were $T_{1a} = 2$ s, $T_{2a} = 0.2$ s, $T_{1b} = 0.1$ s, $T_{2b} = 0.1$ s, $C_b = 1000$ s^{-1}, and $M_0^b/M_0^a = 0.0003636$. The "true" bound proton lifetime is 1 ms.

fixed to the experimental value (2 s). The results of the fitting for each applied B_1 value are summarized in Table 1. The Eu^{3+}-bound water lifetimes (τ_{MB}) obtained in the fitting procedure were 93, 106, 92, and 67 μs for B_1 values of 109, 229, 505, and 1020 Hz, respectively. These values are comparable to values measured experimentally by more direct NMR methods (22–24). The decrease in estimated τ_{MB} values with increasing B_1 likely reflects a slight warming of the sample using the higher applied B_1. Although the individual estimated lifetimes (τ_{MC}) for the amide protons were within the previously observed range (100–9000 μs) (25), the trend with increasing B_1 values was opposite that found for τ_{MB}. A reasonable explanation is that since the chemical shift of the exchanging NH protons is close to bulk water ($\delta_{NH} \sim -6$ ppm), only a small shoulder can be observed in the CEST spectrum at the lowest B_1 only. This poorly resolved feature results in a substantial error in the estimated lifetimes of the amide protons. This suggests that it is important to use a range of B_1 values, including small values, and sufficiently small irradiation frequency intervals so as to reveal as much information as possible about exchanging sites near the bulk water frequency.

CONCLUSIONS

The use of Cramer's rule to obtain the exact numerical solutions to the steady-state Bloch equations modified for chemical exchange provides a powerful, facile means of fitting CEST spectra from experiments involving multiple types of exchangeable protons. The applied B_1, proton exchange rates, and relaxation times of the bulk solvent are shown to be of primary importance in generating a large CEST effect, and it has also been shown that the magnitude of the CEST effect is relatively insensitive to the relaxation times of the bound exchanging protons. The large chemical shifts associated with PARACEST agents allow for faster proton exchange and hence an increased CEST effect

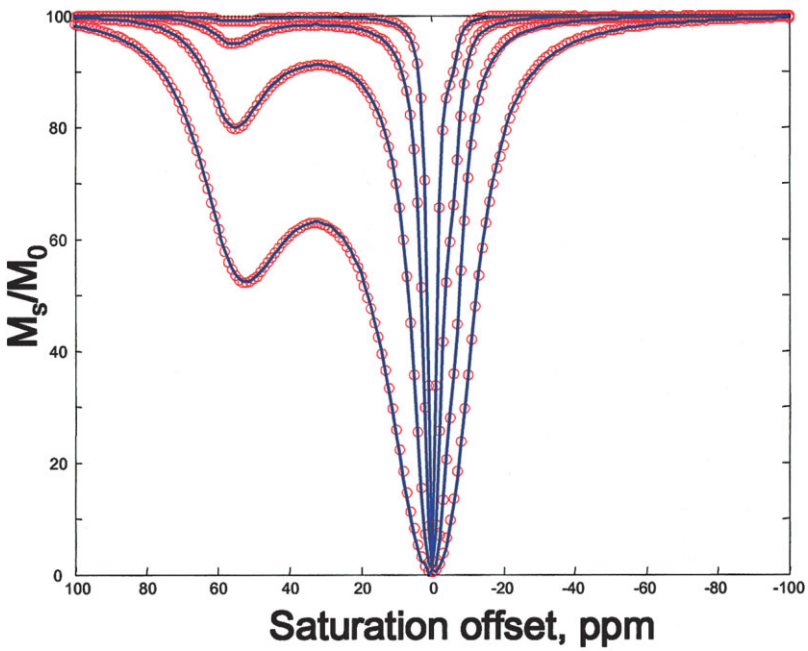

FIG. 7. Experimental CEST spectra (circles) of a 10 mM aqueous solution of EuDOTAM at 4.7 T with B_1 values of 109, 229, 505, and 1020 Hz (in descending order in the graph), respectively. The solid lines are the corresponding best-fitted CEST spectra to the three-pool theory (CESTFIT). The fitted parameters for each curve are reported in Table 1.

15222594, 2005, 4, Downloaded from https://onlinelibrary.wiley.com/doi/10.1002/mrm.20408 by Weizmann Institute Of Science, Wiley Online Library on [26/11/2022]. See the Terms and Conditions (https://onlinelibrary.wiley.com/terms-and-conditions) on Wiley Online Library for rules of use; OA articles are governed by the applicable Creative Commons License

Table 1
The Fitted Parameters for CEST Spectra of 10 mM EuDOTAM Collected Using Different B_1 Values (see Fig. 7)*

Optimized parameters	B_1 = 109 Hz	B_1 = 229 Hz	B_1 = 505 Hz	B_1 = 1020 Hz
τ_{MB}, μs	93	106	92	67
τ_{MC}, μs	382	359	875	1500
δ_B, ppm	56.7	56.6	56.5	55.5
δ_C, ppm	−6.1	−6.3	−6.8	−7.6
T_{1A}, s	2.07	2.23	2.86	3.66
T_{2A}, s	0.88	0.62	0.96	1.50
AF[a]	0.002	0.002	0.004	0.005

*The separate optimizations permitting the relaxation times of the bound pools (T_{1B}, T_{2B}, T_{1C}, and T_{2C}) to vary freely within 0.01 to 5 s gave very similar results. The presaturation pulse length was fixed to 2 s in all cases.

[a]Agreement factor, $AF = \sqrt{\frac{\Sigma(CEST_{exp} - CEST_{cal})^2}{\Sigma CEST_{exp}^2}}$

for a given concentration of PARACEST agent. This feature is highly advantageous for enhancing the sensitivity of exogenous PARACEST agents. This positive feature of PARACEST is partially negated by the fact that faster proton exchange also results in exchange broadening of the bound resonance, which in turn requires a larger B_1 value to reach a given saturation level of the bound proton. Larger B_1 values in turn can result in a greater off-resonance excitation that acts to obscure the true CEST effect in a quantitative sense; therefore, each of these factors (large chemical shift, faster exchange, applied B_1, and off-resonance excitation) must be balanced to yield the greatest CEST effect per unit concentration of PARACEST agent with the least impact of off-resonance excitation.

Equation [23], which is commonly used to estimate the magnitude of the CEST effect, assumes complete saturation of the exchanging bound protons. However, for systems undergoing exchange at moderate rates, this condition may be difficult to achieve experimentally, especially in situations where applied RF power may be limited by sample considerations. The simulations presented here show that incomplete saturation at the exchanging site can result in large errors in parameters as estimated by Eq. [23]. Similarly, Eq. [28] assumes complete saturation of the bound protons and is frequently used to estimate the lifetime of the bound protons. This too results in large errors in parameter estimates for an exchanging system. The ability to calculate and display the degree of saturation of the bound protons enables one to assess the applicability of this limiting case to any given set of NMR parameters and B_1 value.

The use of Cramer's rule and ODE solvers enables one to easily calculate CEST spectra for a wide variety of situations described by the modified Bloch equations, including PARACEST agents and diamagnetic CEST agents. Since no algebraic simplifications of the modified Bloch equations are made, the values of the parameters are constrained only by the physics of the system. This numerical approach enables one to straightforwardly treat complex exchange pathways and multipool systems; for example, four-pool systems have been measured and analyzed (unpublished results). An apparent disadvantage of the present numerical approach is that it does not result in exact analytical solutions in the form of simple equations. Zhou and coworkers (14) obtained concise analytical solutions for the two-pool CEST case after they made some assumptions and approximations. Their model assumes that only the bound protons are irradiated and that they reach steady-state saturation instantly after RF irradiation. However, we have shown here that saturation of site B protons with a relatively small applied B_1 results in significant off-resonance saturation of site A protons only 475 Hz away from site B protons. Thus, an assumption of site-selective irradiation is likely not valid in most instances. Furthermore, even the simple PARACEST agent used here involves three exchanging pools of protons (one highly shifted and another nearly overlapping the bulk water pool). Thus, a simple two-pool model cannot adequately predict the full CEST spectrum in an experiment involving a PARACEST agent. The present models suggest it is unlikely that the CEST spectrum of a tissue sample with multiple exchanging pools of protons is adequately described by a model involving only two exchanging pools. Although only numerical results are obtained in the present case, the method used to fit experimental CEST spectra here does not require an assumption of instantaneous saturation or attainment of steady state (14), and therefore yields fitted NMR parameters that are subject only to experimental uncertainties and not to errors introduced by the assumptions and approximations of other models (14). For the class of PARACEST agents treated in this paper, the CEST spectra are relatively insensitive to changes in the bound water proton NMR relaxation times within a wide range of values. This may not be true for CEST agents that have considerably different bound proton lifetimes and relaxation times. Nevertheless, this phenomenon is an important factor in designing PARACEST agents of the present type. A nonlinear least-square optimization to fit CEST data to theory can provide values of pertinent NMR parameters that can aid in the design of optimal PARACEST agents for specific applications.

REFERENCES

1. Caravan P, Ellison JJ, McMurray TJ, Lauffer RB. Gadolinium(III) chelates as MRI contrast agents: structure, dynamics, and applications. Chem Rev 1999;99:2293–2352.
2. Ward KM, Aletras AH, Balaban RS. A new class of contrast agents for MRI based on proton chemical exchange dependent saturation transfer (CEST). J Magn Reson 2000;143:79–87.
3. Goffeney N, Bulte JWM, Duyn J, Bryant LH, van Zijl PCM. Sensitive NMR detection of cationic-polymer-based gene delivery systems using saturation transfer via proton exchange. J Am Chem Soc 2001;123:8628–8629.

15222594, 2005, 4, Downloaded from https://onlinelibrary.wiley.com/doi/10.1002/mrm.20408 by Weizmann Institute Of Science, Wiley Online Library on [26/11/2022]. See the Terms and Conditions (https://onlinelibrary.wiley.com/terms-and-conditions) on Wiley Online Library for rules of use; OA articles are governed by the applicable Creative Commons License

4. Zhou J, Payen J-F, Wilson DA, Traystman RJ, van Zijl PCM. Using the amide proton signals of intracellular proteins and peptides to detect pH effects in MRI. Nat Med 2003;9:1085–1090.
5. Zhou JY, Lal B, Wilson DA, Laterra J, van Zijl PCM. Amide proton transfer (APT) contrast for imaging of brain tumors. Magn Reson Med 2003;50:1120–1126.
6. Zhang S, Winter P, Wu K, Sherry AD. A novel europium(III)-based MRI contrast agent. J Am Chem Soc 2001;123:1517–1518.
7. Sherry AD, Zhang S, Wu K. Paramagnetic metal ion-based macrocyclic magnetization transfer contrast agents and method of use. WO 0243775 patent 0243775; 2002.
8. Zhang S, Sherry AD. Physical characteristics of lanthanide complexes that act as magnetization transfer (MT) contrast agents. J Solid State Chem 2003;171:38–43.
9. Aime S, Barge A, Castelli DD, Fedeli F, Mortrillaro A, Nielsen FU, Terreno E. Paramagnetic Lanthanide(III) complexes as pH-sensitive chemical exchange saturation transfer (CEST) contrast agents for MRI application. Magn Reson Med 2002;47:639–648.
10. Aime S, Castelli DD, Terreno E. Novel pH-reporter MRI contrast agents. Angew Chem Int Ed 2002;41:4334–4336.
11. Aime S, Castelli DD, Fedeli F, Terreno E. A paramagnetic MRI-CEST agent responsive to lactate concentration. J Am Chem Soc 2002;124: 9364–9365.
12. Zhang S, Trokowski R, Sherry AD. A paramagnetic CEST agent for imaging glucose by MRI. J Am Chem Soc 2003;125:15288–15289.
13. Zhang S, Merritt M, Woessner DE, Lenkinski RE, Sherry AD. PARACEST agents: modulating MRI contrast via water proton exchange. Accts Chem Res 2003;36:783–790.
14. Zhou J, Wilson DA, Sun PZ, Klaus JA, Van Zijl PCM. Quantitative description of proton exchange processes between water and endogenous and exogenous agents for WEX, CEST, and APT experiments. Magn Reson Med 2004; 51:945–952.
15. McConnell HM. Reaction rates by nuclear magnetic resonance. J Chem Phys 1958;28:430–431.
16. Woessner DE. Nuclear transfer effects in nuclear magnetic resonance pulse experiments. J Chem Phys 1961;35:41–48.
17. Reeves LW, Shaw KN. Nuclear magnetic resonance studies of multi-site chemical exchange. I. Matrix formulation of the Bloch equations. Can J Chem 1970;48:3641–3653.
18. Hall C, Kydon DW, Richards RE, Sharp RR. Multisite chemical exchange effects in the NMR spectra of quadrupolar nuclei; the aqueous chloride/chlorine system as an example. Proc R Soc Lond Ser A: Math Phys Eng Sci 1970;318:119–141.
19. Noggle JN. QuickBasic programming for scientists and engineers. Boca Raton, FL: CRC Press, Inc.; 1992. 337 p.
20. Amin S, Morrow JR, Lake CH, Churchill MR. Complexes from lanthanide(III) ions and macrocyclic tetraamides as synthetic ribonucleases: structure and catalytic properties of [La(tcmc)(CF_3SO_3)(EtOH)] (CF_3SO_3)$_2$. Angew Chem Int Ed 1994;33:773–775.
21. Bloch F. Nuclear induction. Phys Rev 1946;70:460–474.
22. Aime S, Barge A, Botta M, De Sousa AS, Parker D. Direct NMR spectroscopic observation of a lanthanide-coordinated water molecule whose exchange rate is dependent on the conformation of the complexes. Angew Chem Int Ed 1998;37:2673–2675.
23. Dunand FA, Aime S, Merbach AE. First ^{17}O NMR observation of coordinated water on both isomers of [Eu(DOTAM)(H_2O)]$^{3+}$: a direct access to water exchange and its role in the isomerization. J Am Chem Soc 2000;122:1506–1512.
24. Zhang S, Michaudet L, Burgess S, Sherry AD. The amide protons of an ytterbium(III) dota tetraamide complex act as efficient antennae for transfer of magnetization to bulk water. Angew Chem Int Ed 2002;41: 1919–1921.
25. Zhang S, Sherry AD. Paramagnetic CEST agents: NH *versus* OH. In: Proceedings of the 10th Annual Meeting of ISMRM, Honolulu, 2002. p 2590.

15222594, 2005, 4, Downloaded from https://onlinelibrary.wiley.com/doi/10.1002/mrm.20408 by Weizmann Institute Of Science, Wiley Online Library on [26/11/2022]. See the Terms and Conditions (https://onlinelibrary.wiley.com/terms-and-conditions) on Wiley Online Library for rules of use; OA articles are governed by the applicable Creative Commons License